To be published in Optical Materials Express:

Title: Wavelength-Dependent Multifunctional Metalens Devices via Genetic Optimization

Authors: Jianzheng Ren,Tianyue Li,Boyan Fu,Shuming Wang,Zhenlin Wang,Shining Zhu

Accepted: 12 October 21

Posted 14 October 21

DOI: https://doi.org/10.1364/OME.442605

Wavelength-Dependent Multifunctional Metalens Devices via Genetic Optimization

JIANZHENG REN,[1] TIANYUE LI,[1] BOYAN FU,[1] SHUMING WANG,[1,2,*] ZHENLIN WANG,[1] AND SHINING ZHU[1,2]

[1]*National Laboratory of Solid-State Microstructures, Collaborative Innovation Center for Advanced Microstructures, School of Physics, Nanjing University, Nanjing, 210093, China.*

[2]*Key Laboratory of Intelligent Optical Sensing and Manipulation Ministry of Education, Nanjing 210093, China.*

[*]*wangshuming@nju.edu.cn.*

Abstract: Metalenses with non-trivial performance, abundant applications and tremendous potentials have emerged as a flat optical element or configuration in recent years. The increasing concerns about how to integrate more functions into a single metalens have become a hot topic. Here, based on genetic algorithm, we demonstrate several metalenses with more than two optical functions depending on the wavelength of light. We first design three arbitrary chromatic dispersive metalenses, whose focal planes can be determined at will at different wavelengths. Then, a metalens-based color router is presented, which is able to guide and focus the light with four wavelengths to different positions. Furthermore, we exhibit a tri-functional structured light generator to produce focused beam, focused orbital angular momentum beam and the Bessel beam at three wavelengths, respectively. Our results may have potential applications in dispersion manipulation, optical micro-manipulation and subwavelength resolution spectral imaging.

1. Introduction

Traditional optical elements or configurations are gradually replaced by planar diffractive elements (PDEs) due to their bulky size and complex system. As one of the promising PDEs, metasurface, consisting of the array of subwavelength nano-units, plays a crucial role during the last decade, especially metalenses, which can not only realize diffraction-limit focusing and full-color imaging but also attribute to their compact volumes [1-5]. Fundamental strategies of metalens design mainly classify into three types. Among them, most of works are based on the geometrical (Pancharatnam-Berry) phase for circularly polarization operation, some are dependent on propagation phase in dielectric waveguide segments and others are follows by multiple resonance on the unit cell[6]. Meanwhile, increasing metasurface devices arise in the field of quantum source [7, 8], nonlinear optics[9, 10] and other specific applications like spectroscopies [11], endoscopes [12] and meta-fibers [13].

The other major superiority of metalenses is their multifunctionality. Precisely manipulating multidimensional optical parameters of light field can achieve different phase or amplitude distributions. For example, orthogonal polarizations are important parameters of light that can be completely implemented to realize absolutely independent phase profiles [13-19]. By designing the metalens with different incident angles, various optical responses can also be obtained in the reflection plane [20]. Therefore, how to further add more functionalities in a single-layer metasurface has a strong appeal to the researchers. Theoretically, wavelengths have unlimited capability, which has been demonstrated on a reflective metasurfaces in the previous work [21], but fail to perform the transmissive functionalities owing to its reflection. Besides, the metalens reported by another work has achieved only two kinds of light-field manipulation within a certain bandwidth and cannot be polarization-insensitive [22], which greatly impacts the multiplexing of metalens. Here, we design the multifunctional metalenses to realize two more functionalities at corresponding wavelengths through arranging three kinds of centrosymmetric nanopillars with polarization-independent features by genetic algorithm in the near-infrared regime. Through this scheme, arbitrary focal planes at different wavelengths incidence can be achieved and two meta-devices named color router and tri-functional structured light generator are revealed, respectively. This work is a further extension of dispersion-engineering and we envision it to occupy a position in multifunctional optical platforms.

2. Principle of metalens design

Our design principle is mainly implemented by the appropriate arrangement of three centrosymmetric dielectric nanopillars, whose phase shifts depends on the propagation phase with polarization-independent property, therefore, a phase library of nanopillars to realize the required phase shifts should be built. In this work, we design three basic structures labeled as A, B and C to cover 0-2π in phase space, which is shown in Fig.1(a). These centrosymmetric nanopillars composed of silicon (Si) on a fused silica (SiO_2) substrate can be considered as truncated waveguides[23] because of the high-index contrast between the nanopillar (n_{Si}=3.48) and air (n_{air}=1). Finite-difference time domain (FDTD) simulations are performed to acquire phase shifts of nanopillars for 5 nm increment of each geometric parameter by using the commercial software package "FDTD Solutions" (Lumerical Inc.). Periodic boundary conditions are applied along the x and y axes, and the perfectly matched layers (PMLs) are applied to the z direction. The sweeping scope of lengths (L) and widths (W) of the nanopillars covers 50 nm to 600 nm with fixed Height (H) H = 1 μm, and the properly arranged array of nanopillars have a lattice constant of $P_x = P_y$ = 600 nm. The results of phase shifts of all the nanopillars for four wavelengths spread out on the entire 2π × 2π squire, which are illustrated in Fig.1(b).

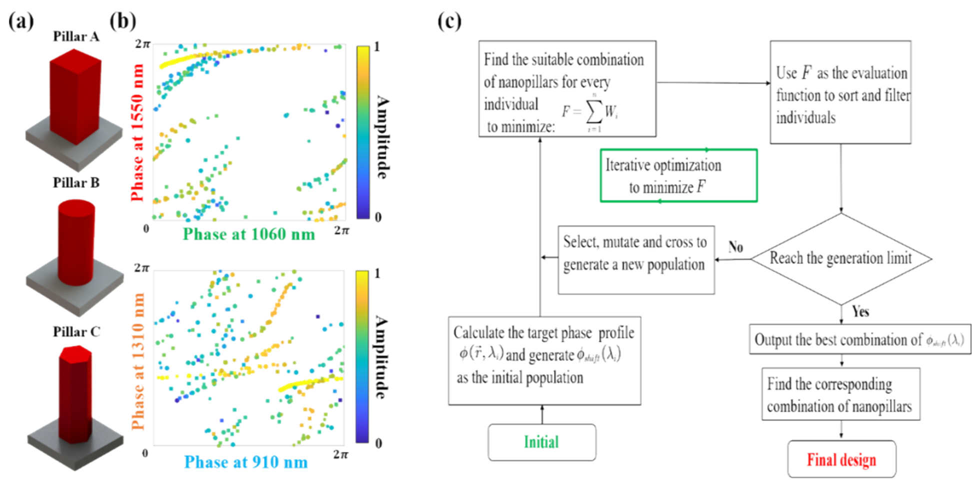

Fig. 1. (a). Typical nanopillars of our design. (b). Phase library of nanopillars for four wavelengths response in the 2π × 2π phase space, square, circular and star points corresponds to the designed pillar A, B and C (phase shifter). Color map represents the amplitudes of typical pillars. (c). Flow chart of genetic algorithm optimization applied in design principle.

The independent phase shifts for each wavelength provide possibility to realize multifunctional devices. However, it can be seen from Fig. 1(b) that the phase shifts cannot exactly cover every corner of the phase space, and it still requires larger phase space to successfully realize the required metalens. Therefore, the optimization of genetic algorithm has been chosen for the suitable arrangement of nanopillars, and $\Phi_{\mathrm{shift}}(\lambda_i)$ is introduce as a constant value to amend and optimize the phase profile, which is unable to impact the objective functions for it only changes the absolute phase of every λ_i instead of relative phase. The $\varphi_i(x, y, \lambda_i)$ represents the target phase at the coordinate (x, y) for wavelength λ_i, and $\varphi_{\mathrm{real}}(x, y, \lambda_i)$ is the phase saved in the library of the chosen pillar at the specific site (x, y). In order to get the optimized $\Phi_{\mathrm{shift}}(\lambda_i)$ for every λ_i [24], we choose to adopt the genetic algorithm. We first define the residue function R_i, which is used to measure the matching degree between the real phase $\varphi_{\mathrm{real}}(x, y, \lambda_i)$ and the adjusted target phase profile $\varphi_i(x, y, \lambda_i) + \Phi_{\mathrm{shift}}(\lambda_i)$. R_i is defined as:

$$R_i = \sum_{j=1}^{N} \left| e^{i\varphi_{\mathrm{real}}(\vec{x},\vec{y},\lambda i)} - e^{i[\varphi_i(\vec{x},\vec{y},\lambda i)+\phi_{\mathrm{shift}}(\lambda_i)]} \right| \tag{1}$$

where N is the number of nanopillars placed in the metalenses. Considering that different functions have different tolerances to residuals, we introduce weighted residue function W_i as:

$$W_i = \beta_i R_i = \beta_i \sum_{j=1}^{N} \left| e^{i\varphi_{\mathrm{real}}(\vec{x},\vec{y},\lambda i)} - e^{i[\varphi_i(\vec{x},\vec{y},\lambda i)+\phi_{\mathrm{shift}}(\lambda_i)]} \right| \tag{2}$$

where β_i represents a parameter weighing the tolerance to residues requiring multiple adjustments based on simulation results. Clearly, the high βi means the low tolerance to residues for function i. The genetic algorithm to determine $\Phi_{\text{shift}}(\lambda_i)$ is applied for every λ_i. Here, the fitness function F can be defined as:

$$F=\sum_{i=1}^{n} W_i = \sum_{i=1}^{n} \beta_i \sum_{j=1}^{N} \left| e^{i\varphi_{\text{real}}(\vec{x},\vec{y},\lambda i)} - e^{i[\varphi_i(\vec{x},\vec{y},\lambda i)+\phi_{\text{shift}}(\lambda_i)]} \right| \tag{3}$$

where n denotes the number of working wavelengths. Using the $\Phi_{\text{shift}}(\lambda_i)$ produced by the genetic algorithm, the best arrangement of nanopillars to minimize the fitness function F can be obtained. The flow chart of optimization based on genetic algorithm is shown in Fig.1(c). Subsequently, the simulation of objective metalenses has been numerically demonstrated by adjusting β_i according to the results, until all target functionalities can be simultaneously achieved.

3. Result and discussion

3.1 Chromatic dispersion manipulation

The left parts of Figure. 2(a)-(c) schematically show the three metalenses (R=8 μm) that arbitrarily control chromatic dispersion at four wavelengths in the near-infrared regime (910nm, 1060nm, 1310nm, 1550nm). As a verification of our design scheme, metalens 1 exhibits achromatic focusing at f=15 μm for all four wavelengths, and metalens 2 displays achromatic capabilities with separate focal lengths for 1550 nm and 1310 nm at f_1=15 μm, 1060 nm and 910 nm at f_2=9 μm, respectively. While metalens 3 employs another situation that 1550 nm and 1060 nm focus at f_1=15 μm and 1310 nm and 910 nm focus at f_1=9 μm. The corresponding phase profiles of our design with double focal lengths characteristics satisfy the following functions:

$$\varphi_1(x,y,\lambda_i) = -\frac{2\pi}{\lambda_i}\left(\sqrt{x^2+y^2+f_1^2} - f_1\right) \tag{4}$$

$$\varphi_2(x,y,\lambda_i) = -\frac{2\pi}{\lambda_i}\left(\sqrt{x^2+y^2+f_2^2} - f_2\right) \tag{5}$$

where λ_i is the design wavelength, (x, y) represents the position of each nanopillar on the metalenses, f_1 and f_2 are the focal lengths. Note that when f_1=f_2=15 μm, the achromatic metalens can be satisfied.

The middle parts of Fig.2 (a)-(c) is the optimal configuration of the metalens. The right parts show the simulation results of the corresponding ones, with the four wavelengths colored as red (1550 nm), yellow (1310 nm), green (1060 nm) and blue (910 nm) for vivid visualization, which shows the longitudinal intensity distributions and transvers patterns with full-width at half minimum (FWHM) from top to bottom. The corresponding values are shown in Table 1. One can see that the focal planes are in agreement with theoretical expectation, proving that we successfully control the chromatic aberration as expected. In theory, we can realize arbitrary chromatic aberration with this method by replacing the phase profiles with the target profiles. Here, we only demonstrate three typical instances as a proof of principle.

Note that the demonstration is only guaranteed for several discrete wavelengths, which is distinguished from previous reports on achromatic metalenses design within a continuous spectral bandwidth. [1-4,6,22,25,26]

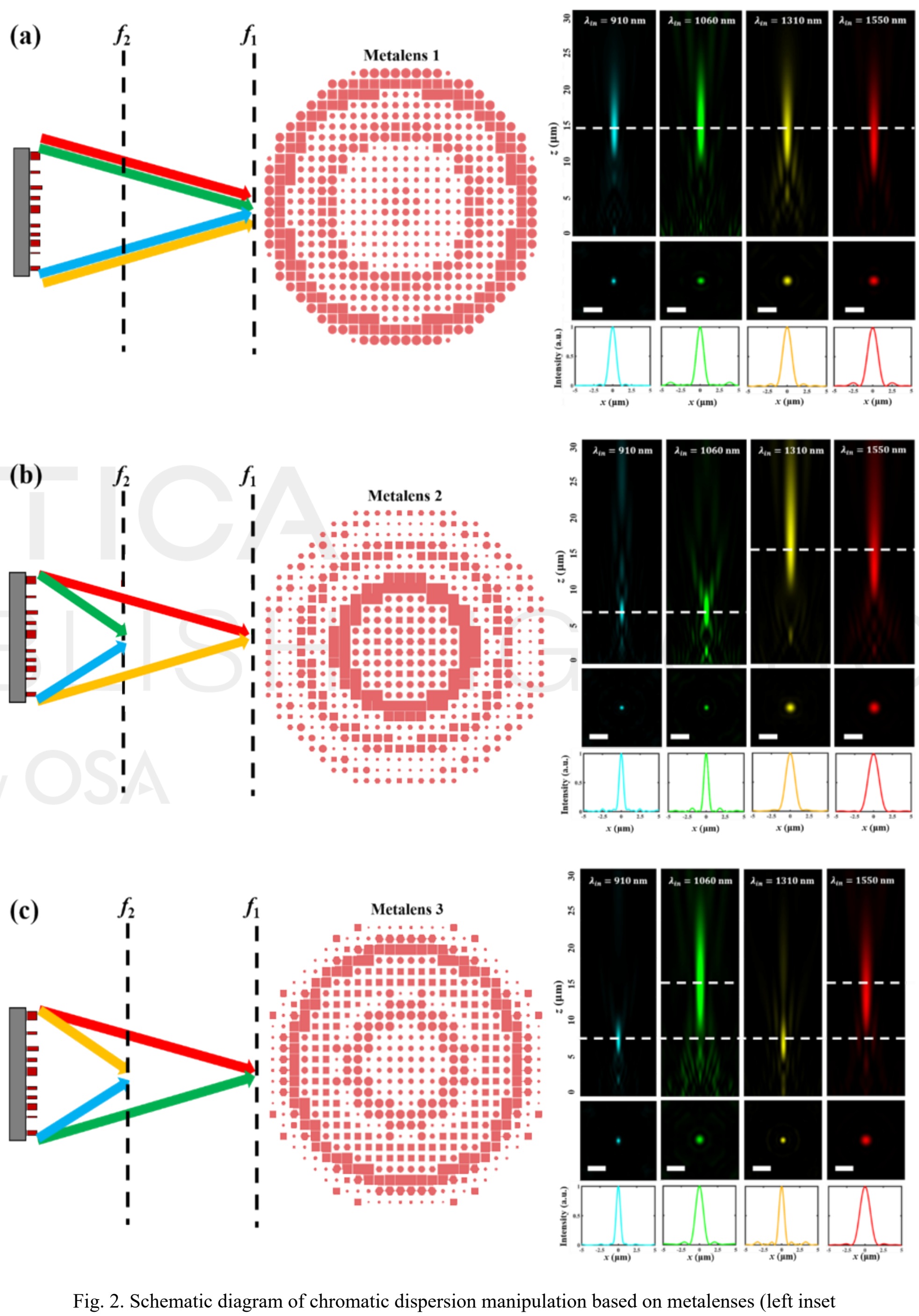

Fig. 2. Schematic diagram of chromatic dispersion manipulation based on metalenses (left inset in (a), (b) and (c)), configuration of metalenses (middle inset in (a), (b) and (c)) and simulated

longitudinal intensity distributions, transverse intensity distributions (scale bar: 2μm) with corresponding FWHMs (from top to bottom, right inset in (a), (b) and (c)).

Wavelength (nm)	Metalens sample	Efficiency (%)	FWHM (μm)
	1	29.5	1.052
910	2	38.2	0.648
	3	40.2	0.665
	1	24.1	1.087
1060	2	34.6	0.687
	3	35.8	1.232
	1	42.7	1.289
1310	2	51.4	1.399
	3	45.1	0.826
	1	61.4	1.509
1550	2	46.7	1.646
	3	63.5	1.608

Table 1. The efficiency and FWHM of Metalens sample 1, 2, 3. The efficiency is defined as the ratio of the power of the spot at the focal plane to incident power.

3.2 Metalens-Based Color Router

Wavelengths providing information in the spectral domain have been applied in material composition, temperature [27-29] and exoplanet search [30], which is recorded by the integration of a conventional Bayer-filter with CCD/CMOS [31]. The emergence of metalens-based color router (Meta-CR) is expected to overcome various aligned lithography steps for their manufacture with lower miniaturization, however, this geometric phase-based device requires circularly polarized light incident, which hinders its practical development [32].

Based on the discussion above, a polarization-independent Meta-CR has been proposed by our method, whose schematic diagram is depicted in Figure 3(a). The required phase profile can be written as:

$$\varphi_{\mathrm{MBCR}}(x, y, \lambda_i) = -\frac{2\pi}{\lambda_i}\left(\sqrt{(x+\Delta x)^2+(y+\Delta y)^2+f^2}-f\right)+\phi_{\mathrm{shift}}(\lambda_i) \tag{6}$$

where $\triangle x$ and $\triangle y$ are offset distance of the focal position. In our design, the offset distance from the center of each spot is set as 2 μm. Fig.3(b) gives the configuration of a 10 μm × 10 μm polarization-independent Meta-CR and the simulation results are shown in Fig. 3(c) and (d), which can vividly show the situation when light containing the four wavelengths simultaneously incident. The efficiencies are 23.4% (910 nm), 28.9% (1060 nm), 28.0% (1310 nm) and 42.4% (1550nm) for multiwavelength incident, respectively.

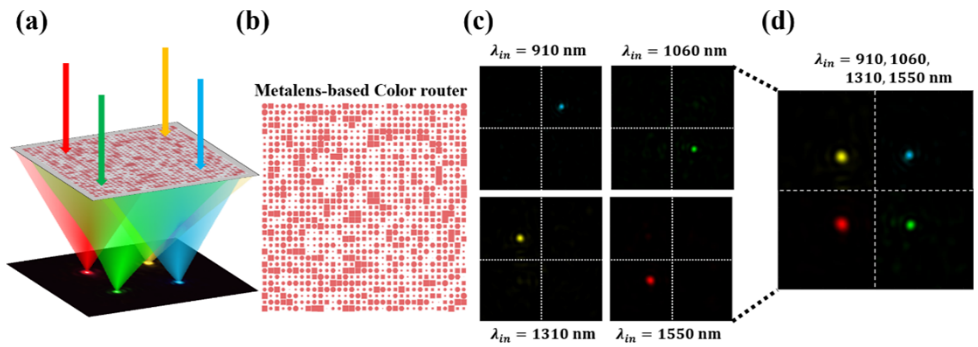

Fig. 3. (a). Schematic diagram of metalens-based color router. (b). Configuration of Meta-CR. (c), (d). Simulated transverse intensity distributions with four wavelengths incident simultaneously, scale bar: 2μm.

3.3 Tri-functional structured light generator

Structured light plays a significant role in the fields of microscopy [33, 34], communication [35] and astrophotonics [36]. How to achieve the multifunctional switching and take full advantage of a single-layer structured beam generator is the topic of our concern. For this reason, we select three wavelengths (λ_1=910 nm, λ_2=1060 nm and λ_3=1310 nm) to complete this design.

For a proof-of-concept, a tri-functional metalens-based structured light generator (Figure 4(a)) to generate focused orbital angular momentum (F-OAM) beam, Bessel beam and focused beam has been designed and numerically demonstrated. The phase profile must fulfill the following equations [16, 37]:

$$\varphi_{\mathrm{OAM}}(x,y) = -\frac{2\pi}{\lambda_1}\left(\sqrt{x^2+y^2+f^2}-f\right)+l\theta+\phi^{1}{}_{\mathrm{shift}}(\lambda_1) \tag{7}$$

$$\varphi_{\mathrm{Bessel}}(x,y) = -\frac{2\pi}{\lambda_2}\left(\sqrt{x^2+y^2}\cdot \mathrm{NA}\right)+\phi^{2}{}_{\mathrm{shift}}(\lambda_2) \tag{8}$$

$$\varphi_{\mathrm{focus}}(x,y) = -\frac{2\pi}{\lambda_3}\left(\sqrt{x^2+y^2+f^2}-f\right)+\phi^{3}{}_{\mathrm{shift}}(\lambda_3) \tag{9}$$

where θ=arctan(y/x) is the azimuthal angle, which represents the higher-order light imparted by the optical vortex, and l is the topological charge. NA is the numerical aperture of the metalens. Here, we set l=1 and NA=0.6. The tri-functional metalens samples produced by our optimal design method is illustrated in Fig.4(b), and the simulation results with $\mathrm{FWHM}_1^{optimized}$~0.736 μm, $\mathrm{FWHM}_2^{optimized}$~0.600 μm, $\mathrm{FWHM}_3^{optimized}$~1.348 μm are shown in Fig.4 (c). While for the ideal situation displayed in Fig.4(c), the corresponding results are FWHM_1^{ideal}~0.816 μm, FWHM_2^{ideal}~0.742 μm, FWHM_3^{ideal}~1.300 μm. Compared with the ideal results, the donut shape, Bessel pattern and focal spot are almost the same, FWHM differential of ideal and simulated results are merely 0.080 μm, 0.142 μm and 0.048 μm, proving that the tri- structured light generator is of successfulness and robustness. One can see that the F-OAM beam has donut shape can be observed at λ_1=910 nm incidence, while the generated Bessel beam at λ_2=1060 nm propagates a long distance with a non-diffraction property, and a focused beam for λ_3=1310 nm incidence coverages into a clear spot at the focal plane. The efficiencies for each beam are 28.7%, 43.0% and 36.0%, respectively, and the intensity distribution of the corresponding light fields with less crosstalk can be apparently seen in Fig.4(c).

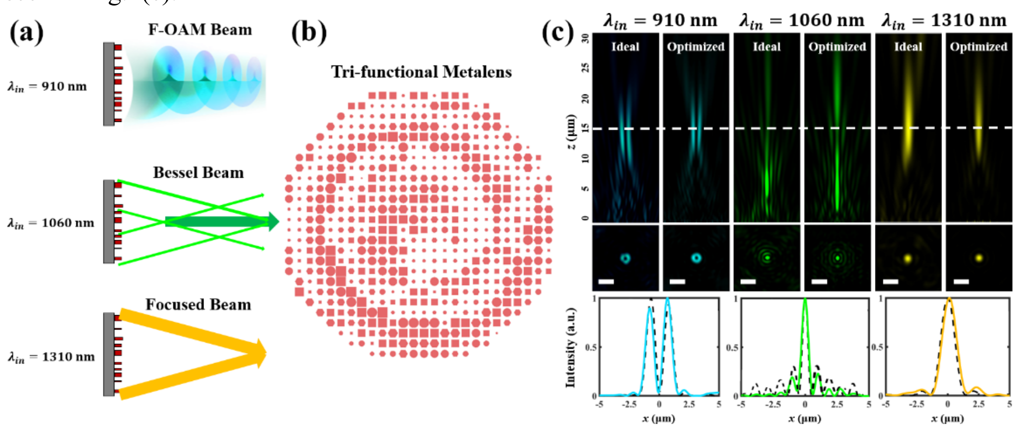

Fig. 4. (a). Schematic diagram of tri-functional metalens-based structured light generator. (b). Configuration of metalens. (c). Comparison of simulated longitudinal intensity distributions, transverse intensity distributions of ideal and optimized results with corresponding FWHMs (from top to bottom). Solid lines represent optimized results; dash lines denote as ideal results. Scale bar: 2μm.

4. Conclusion

In summary, we employ the genetic algorithm optimization to arbitrarily manipulate the chromatic dispersion based on metalenses, and then we design the metalens-based color router in the near infrared region. Finally, we show the multifunctional structured light generator that can modulate more complex phase profiles at different wavelengths. Additionally, the meta-devices in this work possess a polarization-independent property due to the phase library consisting of centrosymmetric nanopillars. Metalens based on the optimization algorithm can not only allow multiple functions by utilizing the dimension of wavelength, but also have the merits of miniaturization and integration, which are expected to apply in the next generation of optical platform. We also anticipate that wavelength-multiplexing multifunctional metalenses have greater potential in computer science.

Funding. The authors acknowledge financial support from the National Program on Key Basic Research Project of China (2017YFA0303700), National Natural Science Foundation of China (no. 11621091, 11822406, 11834007, 11774164, 11774162). This work is also supported by the Fundamental Research Funds for the Central Universities No.020414380175.

Disclosures. The authors declare no conflicts of interest.

Data availability. Data underlying the results presented in this paper are not publicly available at this time but may be obtained from the authors upon reasonable request.

Acknowledgments. The authors are grateful for the help from Quan Yuan, Jun Liu, Run Chen, Xiujuan Zou, Yifan Wu, Xiaoshu Zhu, Guangxing Gong, Ruoyu Lin, Mengjing Xu, Qianhui Bi and Mingqian Shi.

References

1. S. Wang, P. C. Wu, V. C. Su, Y. C. Lai, C. Hung Chu, J. W. Chen, S. H. Lu, J. Chen, B. Xu, C. H. Kuan, T. Li, S. Zhu, and D. P. Tsai, "Broadband achromatic optical metasurface devices," Nature Communications **8**, 187 (2017).
2. W. T. Chen, A. Y. Zhu, V. Sanjeev, M. Khorasaninejad, Z. Shi, E. Lee, and F. Capasso, "A broadband achromatic metalens for focusing and imaging in the visible," Nature Nanotechnology **13**, 220-226 (2018).
3. S. Wang, P. C. Wu, V. C. Su, Y. C. Lai, M. K. Chen, H. Y. Kuo, B. H. Chen, Y. H. Chen, T. T. Huang, J. H. Wang, R. M. Lin, C. H. Kuan, T. Li, Z. Wang, S. Zhu, and D. P. Tsai, "A broadband achromatic metalens in the visible," Nature Nanotechnology **13**, 227-232 (2018).
4. R. J. Lin, V. C. Su, S. Wang, M. K. Chen, T. L. Chung, Y. H. Chen, H. Y. Kuo, J. W. Chen, J. Chen, Y. T. Huang, J. H. Wang, C. H. Chu, P. C. Wu, T. Li, Z. Wang, S. Zhu, and D. P. Tsai, "Achromatic metalens array for full-colour light-field imaging," Nature Nanotechnology **14**, 227-231 (2019).
5. L. Li, Q. Yuan, R. Chen, X. Zou, W. Zang, T. Li, G. Zheng, S. Wang, Z. Wang, and S. Zhu, "Chromatic dispersion manipulation based on metasurface devices in the mid-infrared region," Chinese Optics Letters **18**, 082401 (2020).
6. O. Tsilipakos, M. Kafesaki, E. N. Economou, C. M. Soukoulis, and T. Koschny, Advanced Optical Materials 8 (2020).
7. L. Li, Z. Liu, X. Ren, S. Wang, V.-C. Su, M.-K. Chen, C. H. Chu, H. Y. Kuo, B. Liu, W. Zang, G. Guo, L. Zhang, Z. Wang, S. Zhu, and D. P. Tsai, "Metalens-array–based high-dimensional and multiphoton quantum source," Science **368**, 1487–1490 (2020).
8. Y. Bao, Q. Lin, R. Su, Z.-K. Zhou, J. Song, J. Li, and X.-H. Wang, "On-demand spin-state manipulation of single-photon emission from quantum dot integrated with metasurface," Science Advances **6**, eaba8761 (2020).
9. Z. Qin, H. Chen, T. Hu, M. Zhang, Z. Chen, and Z. Wang, "Enhanced second-harmonic generation from gold complementary split-ring resonators with a dielectric coating," Optics Express **29**, 15269-15278 (2021).
10. G. Li, S. Zhang, and T. Zentgraf, "Nonlinear photonic metasurfaces," Nature Reviews Materials **2**(2017).
11. A. Y. Zhu, W. T. Chen, J. Sisler, K. M. A. Yousef, E. Lee, Y. W. Huang, C. W. Qiu, and F. Capasso, "Compact Aberration-Corrected Spectrometers in the Visible Using Dispersion-Tailored Metasurfaces," Advanced Optical Materials **7**, 1801144 (2018).
12. H. Pahlevaninezhad, M. Khorasaninejad, Y. W. Huang, Z. Shi, L. P. Hariri, D. C. Adams, V. Ding, A. Zhu, C. W. Qiu, F. Capasso, and M. J. Suter, "Nano-optic endoscope for high-resolution optical coherence tomography in vivo," Nature Photonics **12**, 540-547 (2018).

13. E. Nazemosadat, M. Mazur, S. Kruk, I. Kravchenko, J. Carpenter, J. Schröder, P. A. Andrekson, M. Karlsson, and Y. Kivshar, "Dielectric Broadband Metasurfaces for Fiber Mode-Multiplexed Communications," Advanced Optical Materials **7**, 1801679 (2019).
14. S. Li, X. Li, G. Wang, S. Liu, L. Zhang, C. Zeng, L. Wang, Q. Sun, W. Zhao, and W. Zhang, "Multidimensional Manipulation of Photonic Spin Hall Effect with a Single-Layer Dielectric Metasurface," Advanced Optical Materials **7**, 1801365 (2018).
15. P. Huo, C. Zhang, W. Zhu, M. Liu, S. Zhang, S. Zhang, L. Chen, H. J. Lezec, A. Agrawal, Y. Lu, and T. Xu, "Photonic Spin-Multiplexing Metasurface for Switchable Spiral Phase Contrast Imaging," Nano Letters **20**, 2791-2798 (2020).
16. T. Li, X. Li, S. Yan, X. Xu, S. Wang, B. Yao, Z. Wang, and S. Zhu, "Generation and Conversion Dynamics of Dual Bessel Beams with a Photonic Spin-Dependent Dielectric Metasurface," Physical Review Applied **15**, 014059 (2021).
17. T. Li, X. Xu, B. Fu, S. Wang, B. Li, Z. Wang, and S. Zhu, "Integrating the optical tweezers and spanner onto an individual single-layer metasurface," Photonics Research **9**, 1062-1068 (2021).
18. T. Li, B. Fu, J. Ren, S. Wang, Z. Wang, S. Zhu "Multidimensional light field manipulation and applications based on optical metasurface," in First Optics Frontier Conference, (Proc. SPIE 2021), p. 1185004
19. Y. Bao, L. Wen, Q. Chen, C.-W. Qiu, and B. Li, "Toward the capacity limit of 2D planar Jones matrix with a single-layer metasurface," Science Advances **7**, eabh0365 (2021).
20. A. Leitis, A. Tittl, M. Liu, B. H. Lee, M. B. Gu, Y. S. Kivshar, and H. Altug, "Angle-multiplexed all-dielectric metasurfaces for broadband molecular fingerprint retrieval," Science Advances **5**, eaaw2871 (2019).
21. Z. Shi, M. Khorasaninejad, Y. W. Huang, C. Roques-Carmes, A. Y. Zhu, W. T. Chen, V. Sanjeev, Z. W. Ding, M. Tamagnone, K. Chaudhary, R. C. Devlin, C. W. Qiu, and F. Capasso, "Single-Layer Metasurface with Controllable Multiwavelength Functions," Nano Letters **18**, 2420-2427 (2018).
22. J. Sisler, W. T. Chen, A. Y. Zhu, and F. Capasso, "Controlling dispersion in multifunctional metasurfaces," APL Photonics **5**, 056107 (2020).
23. A. Arbabi, Y. Horie, M. Bagheri, and A. Faraon, "Dielectric metasurfaces for complete control of phase and polarization with subwavelength spatial resolution and high transmission," Nature Nanotechnology **10**, 937-943 (2015).
24. D. E. Goldberg, *Genetic Algorithms in Search, Optimization, and Machine Learning* (Addison-Wesley Publishing Company, Inc., 1989).
25. O. Tsilipakos, L. Zhang, M. Kafesaki, C. M. Soukoulis, and T. Koschny, ACS Photonics 8, 1649-1655 (2021).
26. Y. Wang, Q. Chen, W. Yang, Z. Ji, L. Jin, X. Ma, Q. Song, A. Boltasseva, J. Han, V. M. Shalaev, and S. Xiao, Nat Commun 12, 5560 (2021).
27. P. Wang and R. Menon, "Ultra-high-sensitivity color imaging via a transparent diffractive-filter array and computational optics," Optica **2**, 933-939 (2015).
28. N. Dean, "Colouring at the nanoscale," Nature Nanotechnology **10**, 15-16 (2015).

29. Y. Yu, L. Wen, S. Song, and Q. Chen, "Transmissive/Reflective Structural Color Filters: Theory and Applications," Journal of Nanomaterials **2014**, 1-17 (2014).

30. Y. Wu, S. Chen, P. Wang, S. Zhou, Y. Feng, W. Zhang, and R. Wei, "Simulation and analysis of the coherent-dispersion spectrometer for exoplanet detection," Monthly Notices of the Royal Astronomical Society **503**, 3032 - 3043 (2021).

31. B. E. Bayer, "Colour imaging array - has mosaic of selectively transmissive filters superposed in registration with solid state array," (July 20, 1976).

32. B. H. Chen, P. C. Wu, V. C. Su, Y. C. Lai, C. H. Chu, I. C. Lee, J. W. Chen, Y. H. Chen, Y. C. Lan, C. H. Kuan, and D. P. Tsai, "GaN Metalens for Pixel-Level Full-Color Routing at Visible Light," Nano Letters **17**, 6345-6352 (2017).

33. L. Gao, L. Shao, B. C. Chen, and E. Betzig, "3D live fluorescence imaging of cellular dynamics using Bessel beam plane illumination microscopy," Nature Protocol **9**, 1083-1101 (2014).

34. S. W. Hell and J. Wichmann, "Breaking the diffraction resolution limit by stimulated emission: stimulated-emission-depletion fluorescence microscopy," Optics Letters **19**, 780-782 (1994).

35. S. Li, X. Li, L. Zhang, G. Wang, L. Zhang, M. Liu, C. Zeng, L. Wang, Q. Sun, W. Zhao, and W. Zhang, "Efficient Optical Angular Momentum Manipulation for Compact Multiplexing and Demultiplexing Using a Dielectric Metasurface," Advanced Optical Materials **8**, 1901666 (2020).

36. C. Sheng, R. Bekenstein, H. Liu, S. Zhu, and M. Segev, "Wavefront shaping through emulated curved space in waveguide settings," Nature Communications **7**, 10747 (2016).

37. W. T. Chen, M. Khorasaninejad, A. Y. Zhu, J. Oh, R. C. Devlin, A. Zaidi, and F. Capasso, "Generation of wavelength-independent subwavelength Bessel beams using metasurfaces," Light: Sciecnce＆Applications **6**, e16259 (2017).